

Understanding thermal annealing of artificial spin ice

Cite as: APL Mater. 7, 111112 (2019); <https://doi.org/10.1063/1.5126713>

Submitted: 04 September 2019 . Accepted: 28 October 2019 . Published Online: 26 November 2019

Xiaoyu Zhang, Yuyang Lao, Joseph Sklenar, Nicholas S. Bingham, Joseph T. Batley, Justin D. Watts, Cristiano Nisoli, Chris Leighton, and Peter Schiffer 



View Online



Export Citation

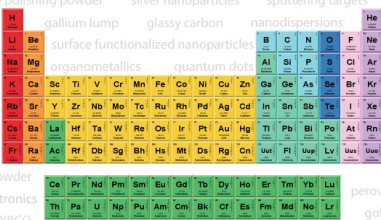


CrossMark



AMERICAN ELEMENTS

THE ADVANCED MATERIALS MANUFACTURER®



additive manufacturing epitaxial crystal growth cerium oxide polishing powder silver nanoparticles sputtering targets III-IV semiconductors CVD precursors europium phosphors

gallium lump glassy carbon nanodispersions InAs wafers laser crystals ultra high purity materials MOFs

surface functionalized nanoparticles organometallics quantum dot rare earth metals photovoltaics refractory metals MOCVD

superconductors transparent ceramics ultra high purity silicon

*American Elements opens up a world of possibilities so you can **Now Invent!***

Over 15,000 certified high purity laboratory chemicals, metals, & advanced materials and a state-of-the-art Research Center. Printable GHS-compliant Safety Data Sheets. Thousands of new products. And much more. All on a secure multi-language "Mobile Responsive" platform.

deposition slugs OLED Lighting spintronics solar energy

osmium nanoribbons thin films chalcogenides AuNPs

GDC Li-ion battery electrolytes 99.999% ruthenium spheres

endohedral fullerenes copper nanoparticles diamond micropowder

CIGS MBE grade materials palladium catalysts flexible electronics

beta-barium borate borosilicate glass dysprosium pellets YBCO

pyrolytic graphite 3d graphene foam indium tin oxide mesoporous silica

raman substrates sapphire windows tungsten carbide InGaAs

barium fluoride carbon nanotubes lithium niobate scandium powder

perovskite crystals yttrium iron garnet alternative energy h-BN

gold nanocubes graphene oxide macromolecules photonics

rhodium sponge fiber optics beamsplitters infrared dyes zeolites

fused quartz metallocenes platinum ink buckyballs Ti-6Al-4V

Now Invent.™

The Next Generation of Material Science Catalogs

www.americanelements.com



Understanding thermal annealing of artificial spin ice

Cite as: APL Mater. 7, 111112 (2019); doi: 10.1063/1.5126713
Submitted: 4 September 2019 • Accepted: 28 October 2019 •
Published Online: 26 November 2019



Xiaoyu Zhang,^{1,2,3} Yuyang Lao,^{2,3} Joseph Sklenar,^{2,3,4} Nicholas S. Bingham,¹ Joseph T. Batley,⁵ Justin D. Watts,^{5,6} Cristiano Nisoli,⁷ Chris Leighton,⁵ and Peter Schiffer^{1,2,3,8,a)} 

AFFILIATIONS

¹Department of Applied Physics, Yale University, New Haven, Connecticut 06511, USA

²Department of Physics, University of Illinois at Urbana-Champaign, Urbana, Illinois 61801, USA

³Frederick Seitz Materials Research Laboratory, University of Illinois at Urbana-Champaign, Urbana, Illinois 61801, USA

⁴Department of Physics and Astronomy, Wayne State University, Detroit, Michigan 48201, USA

⁵Department of Chemical Engineering and Materials Science, University of Minnesota, Minneapolis, Minnesota 55455, USA

⁶School of Physics and Astronomy, University of Minnesota, Minneapolis, Minnesota 55455, USA

⁷Theoretical Division and Center for Nonlinear Studies, MS B258, Los Alamos National Laboratory, Los Alamos, New Mexico 87545, USA

⁸Department of Physics, Yale University, New Haven, Connecticut 06511, USA

^{a)}Electronic mail: peter.schiffer@yale.edu

ABSTRACT

We have performed a detailed study on thermal annealing of the moment configuration in artificial spin ice. Permalloy ($\text{Ni}_{80}\text{Fe}_{20}$) artificial spin ice samples were examined in the prototypical square ice geometry, studying annealing as a function of island thickness, island shape, and annealing temperature and duration. We also measured the Curie temperature as a function of film thickness, finding that thickness has a strong effect on the Curie temperature in regimes of relevance to many studies of the dynamics of artificial spin ice systems. Increasing the interaction energy between island moments and reducing the energy barrier to flipping the island moments allow the system to more closely approach the collective low energy state of the moments upon annealing, suggesting new channels for understanding the thermalization processes in these important model systems.

© 2019 Author(s). All article content, except where otherwise noted, is licensed under a Creative Commons Attribution (CC BY) license (<http://creativecommons.org/licenses/by/4.0/>). <https://doi.org/10.1063/1.5126713>

Artificial spin ice systems are two-dimensional arrays of nanoscale elements, typically composed of single domain ferromagnetic islands.¹ These systems have been the subject of extensive study and have provided models for the study of a range of novel collective behaviors.² Certain artificial spin ice geometries have well-defined collective magnetic ground states, such as the square lattice,¹ while others have intrinsically disordered and complex ground states, such as the Shakti lattice.^{3–5} These low-energy collective states have sparked considerable interest in attempting to realize the lowest energy state of different artificial spin ice lattices.^{6–10} One successful approach to collective energy minimization involves annealing the arrays by heating them to temperatures near or above the Curie temperature (T_C) of the ferromagnetic

material.^{11,12} Upon cooling, the island moments arrange themselves into a low energy state via magnetostatic interactions. Using this method, both long-range-ordered^{11–13} and intrinsically disordered ground states⁴ have been achieved, both in permalloy ($\text{Ni}_{80}\text{Fe}_{20}$) and in other alloys.^{9,10} Notably, the method works well even for geometries known to exhibit slow relaxation toward the low energy state.⁴ Given the high T_C of permalloy, and its importance as a model material for these systems, we investigated thermal annealing of permalloy artificial spin ice by varying the annealing conditions and the geometry of the islands, with the goal of understanding how to improve the effectiveness of annealing.

We fabricated our artificial square spin ice samples on Si wafers coated with a 200-nm-thick layer of Si-N deposited by low

pressure chemical vapor deposition. The nanoislands, with varied lateral dimensions and interisland gaps indicated below, were produced by electron beam lithography and lift-off as described previously.¹² The total area of all nanoislands in each square ice sample was about $200 \times 200 \mu\text{m}^2$. In order to keep uniformity of all nanoislands, the write field for lithography was set to cover the whole sample. We deposited our samples with various thicknesses of permalloy (2–100 nm), and a 3 nm Al cap layer to prevent oxidation, in ultra-high vacuum by molecular beam deposition (using electron beam evaporation). The thickness was established via a quartz-crystal-based rate monitor, which was carefully calibrated by performing grazing-incidence X-ray reflectivity measurements. We performed thermal annealing using a programmable heater (HeatWave Lab) in a vacuum chamber with a base pressure of approximately 10^{-6} Torr in order to prevent sample degradation via oxidation, lateral diffusion, and delamination. After each annealing cycle, we characterized the magnetic state of the arrays in two locations using a magnetic force microscope (MFM), yielding a corresponding microstate map of the arrays. For measurement of T_C of permalloy, we measured the temperature dependence of the magnetization of continuous permalloy films in a superconducting quantum interference device (SQUID) vibrating sample magnetometer (MPMS3 from Quantum Design); the base pressure during T_C measurements was approximately 10^{-3} Torr. The permalloy films used for T_C measurements had an extra 100 nm Si-N encapsulation layer on top, deposited by low pressure chemical vapor deposition to protect them from degradation during the measurements.

The artificial square ice lattice is shown in Fig. 1 with typical SEM (scanning electron microscope) and MFM images shown in Figs. 1(b) and 1(c), respectively. Artificial spin ice systems are often analyzed in terms of the vertices of the lattices, defined as the junctions of multiple islands; the collective magnetic energy is determined to a good approximation by the sum of the magnetostatic energy associated with interactions among the moments at the vertices. The interaction energy between islands can be modified by

varying the island shape and the gap length of the lattice {defined as the edge-to-edge distance between two next nearest neighbor islands [Fig. 1(a)]}.

Each square artificial spin ice vertex consists of four islands with 16 possible magnetic moment configurations [Fig. 1(e)] that can be classified into four types. Unlike the three-dimensional pyrochlore spin ice structure,¹⁴ in which all four spins are equidistant resulting in six degenerate two-in-two-out ground states for each tetrahedron, the two-dimensional square artificial spin ice has four islands that have stronger interactions between the nearest neighbor pairs and weaker interactions between the next nearest neighbor pairs. Therefore, the six-fold ground state degeneracy is broken in square artificial spin ice, and the two type I vertex states are the only ground states for individual vertices. The collective ground state of the system then contains only type I vertices in a long-range-ordered antiferromagnetic configuration.¹⁵ This makes the system ideal for studying the effects of thermal annealing since the ground state fraction provides a clear measure of the effectiveness of annealing.

All annealing treatments on the square ice samples were performed after magnetizing the samples along a 45° angle relative to the lattice to ensure that all the vertices were initially set to a type II state. We then heated the samples to the annealing temperature at a rate of 10 K per minute and held the samples at the annealing temperature for 10 min (unless otherwise stated). Finally, they were cooled at 1 K/min back to 673 K (low enough that the moments were thermally stable) and then quickly cooled to room temperature in about 90 min. For each annealing protocol, we repeated the measurement up to four times. We then measured the effectiveness of annealing for various parameter values, as quantified through the type I vertex population fraction, i.e., the ground state fraction, after annealing.⁹ The error bars below are taken as the standard deviation of vertex fractions from all MFM images. The total number of MFM images for each corresponding data point is two times the number of repeated experiments, as we took two MFM images after

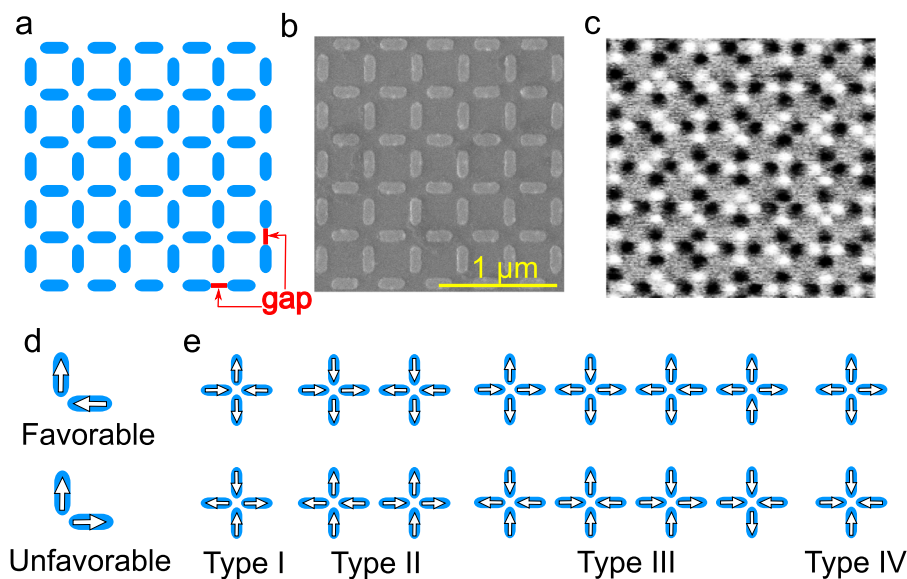


FIG. 1. (a) Schematic of the square artificial spin ice lattice geometry. The gap is defined as the edge-to-edge distance between a pair of next nearest neighbor islands. (b) SEM image and (c) MFM image of the square artificial spin ice lattice. (d) The favorable and unfavorable alignment for moments of the nearest neighbor islands. (e) The energy hierarchy of the vertex types in square artificial spin ice with increasing vertex energy from type I to type IV.

each annealing cycle. Acquired MFM images typically spanned 1700 islands over an area of $15 \times 15 \mu\text{m}^2$.

Since thermal annealing of artificial spin ice moments requires approaching the ferromagnetic T_C , we measured the ferromagnetic moment as a function of temperature in continuous films to determine T_C . In thin film ferromagnetic systems, the second-order transition to the ordered state shows a strong dependence on film thickness associated with finite size scaling,^{16,17} and we thus measured a range of film thicknesses. The magnetization of the films was measured, both zero-field-cooling (ZFC) and field-cooling (FC), as a function of temperature in an in-plane magnetic field of 100 Oe. We estimated T_C as the point of inflection in the magnetization vs temperature curve (raw data used to determine T_C are provided in [supplementary material](#), Fig. SI-1). Although degradation effects such as delamination did not impact our annealing of artificial spin ice samples in high vacuum, we did observe degradation of artificial spin ice samples annealed in the presence of low gas pressures, as in our magnetometer.¹⁸ Notice that we added a Si_3N_4 encapsulation layer on the continuous permalloy film samples used for the T_C measurements to prevent such degradation.

The data in [Fig. 2](#) reveal a strong thickness dependence to T_C , particularly below 10 nm. The inset of [Fig. 2](#) plots the reduction in T_C from bulk (i.e., ΔT_C) vs the thickness. The red line is a fit to the function

$$\frac{T_C(\text{bulk}) - T_C(t)}{T_C(\text{bulk})} = \left(\frac{\xi_0}{t}\right)^\lambda, \quad (1)$$

where t is the thickness of the permalloy film, $T_C(t)$ is the Curie temperature at thickness t , and $T_C(\text{bulk})$ is the Curie temperature of bulk permalloy (taken here to be 820 K¹⁹). The fit gives a correlation length $\xi_0 = 1.48 \text{ nm} \pm 0.11 \text{ nm}$ and a critical shift exponent $\lambda = 1.21 \pm 0.12$, in reasonable agreement with previous measurements

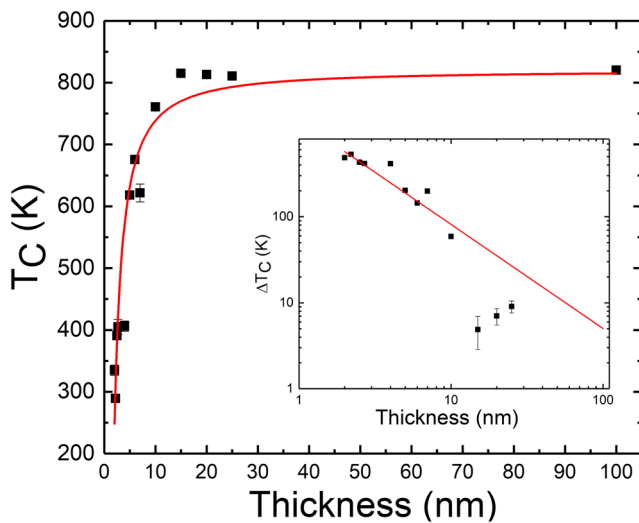


FIG. 2. Thickness dependence of the Curie temperature for permalloy films. The error bars represent the mean absolute error of T_C extracted from ZFC and FC measurements. The red curve shows the fit to Eq. (1). The inset shows the same data, plotted as ΔT_C , which is defined as the difference between the bulk T_C and the measured thin film T_C , assuming a bulk T_C of 820 K.

of ultrathin permalloy films ($\lambda = 1.04$) using spin-polarized cascade electrons.²⁰

This thickness dependence of the permalloy T_C has clear implications for artificial spin ice studies. For example, the suppressed T_C for thinner films is directly relevant to the many photoelectron emission microscopy (PEEM) measurements that have been conducted on permalloy artificial spin ice.^{5,8,21,22} Those measurements focused on films of thickness around 3 nm, and they are therefore conducted relatively close to T_C of the substituent ferromagnetic material. Our data suggest that the observed dynamics in the moment fluctuations might be significantly influenced by the reduced moment associated with the proximity to T_C .

We now discuss studies of annealing while varying different parameters of the lattices and the annealing process. We first describe results of annealing with varying maximum annealing temperature. As the temperature approaches the ferromagnetic transition, the magnetization of permalloy islands decreases, resulting in a decrease in the energy barrier to changing the magnetization orientation of each island along with increased thermal energy in the system. When thermal energy is large enough to overcome the energy barrier required for a moment to switch, the island moments become thermally active and begin to organize themselves into an energetically preferred configuration. The ground-state vertices presumably nucleate in islands with slightly lower energy barriers (potentially associated with imperfections in the lithography) and then expand to large domains. This allows annealing to occur even below T_C of continuous permalloy films.

Our annealing-temperature-dependent data, taken on samples with an island shape of $160 \times 60 \text{ nm}^2$, a gap of 180 nm, and a thickness of 25 nm, are shown in [Fig. 3\(a\)](#), which plots the type-I vertex fraction. As expected, we observed a rather sharp increase in ground state fraction as the temperature is increased toward T_C , with the type I vertex population reaching a maximum at about 83% [see [Figs. 3\(a\)](#) and [3\(e\)](#)] at approximately 790 K. This increase in type-I vertex fraction corresponds to a decrease in the residual polarized vertices as the annealing temperature was increased (see [supplementary material](#), Fig. SI-2). The combination of these data indicates that the moments in the array become thermally active over a range of temperatures. This has the implication that annealing can only succeed in allowing the full system to explore the possible variations in moment configurations by exceeding a certain temperature threshold, where all moments are thermally active. For all data discussed below, there was no significant residual population of the initially polarized vertices, indicating that we exceeded that threshold temperature, and all the moments had the opportunity to thermally fluctuate during the annealing process.

We also examined the dwell time dependence by holding a sample for 10 min, 60 min, or 120 min at an annealing temperature of 773 K or 783 K (data shown in [supplementary material](#), Fig. SI-3). We did not observe any significant effect on the vertex population density, most likely indicating that the system reaches thermal equilibrium on a time scale faster than our experimental temporal resolution, although we cannot rule out the possibility of very slow dynamics associated with long relaxation time scales near the superparamagnetic blocking temperature.

We next investigated the island shape dependence of the ground state fraction after annealing by using a 20-nm-thick sample with island dimensions $160 \times 60 \text{ nm}^2$, $220 \times 60 \text{ nm}^2$, and

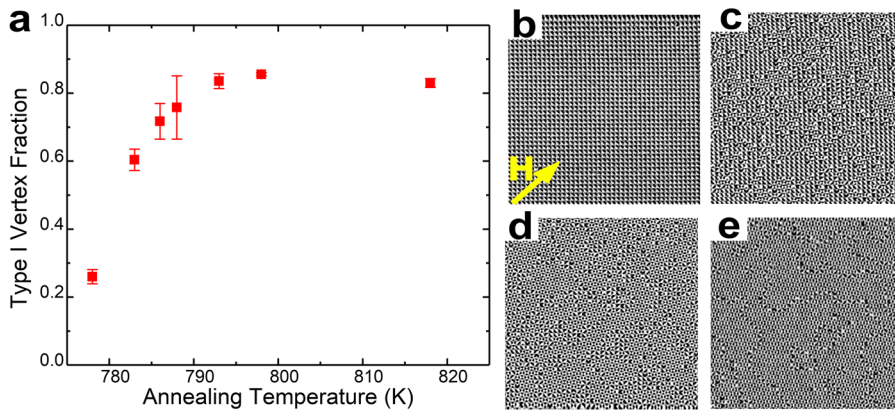


FIG. 3. (a) The ground state fraction as a function of the maximum temperature of annealing for lattices with $160 \times 60 \text{ nm}^2$ island shape, 180 nm gap, and 25 nm thickness. [(b)–(e)] $15 \times 15 \mu\text{m}^2$ MFM images: (b) shows a completely polarized state after a 1000 Oe field was applied along the arrow direction, (c) shows 25% type I vertices after annealing at 778 K, (d) shows 70% type I vertices after annealing at 786 K, and (e) shows 83% type I vertices after annealing at 818 K.

$240 \times 60 \text{ nm}^2$, with gaps of 100 nm, 180 nm, and 280 nm, as shown in Fig. 4. Because these arrays varied in both shape and spacing, we plot the results against the interaction energy between nearest neighbor island pairs, calculated with the micromagnetics code, Object Oriented Micromagnetic Framework (OOMMF),²³ at zero temperature. The samples were annealed at a temperature of 783 K, i.e., below T_C at this thickness. This choice of maximum temperature allowed us to more precisely control the annealing process than would have been possible by annealing above T_C and cooling at rates that necessarily depend on the thermal coupling of the sample to the heater stage. Figure 4(a) presents a plot of type I vertex population fraction vs interaction energy for various island shapes. As previously observed,¹² the ground state fraction is increased with greater interaction strength, a natural consequence of the energy scale of interactions relative to the superparamagnetic blocking temperature. Furthermore, structural disorder intrinsic to lithography will lead to a distribution of both blocking temperature and local interaction strength, which will disrupt the system's ability to reach a collective low-energy state; stronger coupling should overcome this effect.

The annealing process was also more effective with a smaller island aspect ratio. Since these permalloy films have in-plane magnetization and weak magnetocrystalline anisotropy, the aspect ratio dictates the energy barrier to flipping each island moment via shape anisotropy. The energy barrier can be roughly parameterized as

the energy difference between configurations with moments along the long axis and the short axis [Fig. 4(b)]. This energy barrier for each island shape was calculated using MUMAX3²⁴ and is shown in Fig. 4(c) (note that these values are calculated assuming the magnetization at zero temperature). We see that the increase in ground state fraction indeed corresponds to the decrease in this energy barrier. We obtained qualitatively consistent results for two series of islands with 80 nm width and varying length, suggesting that the lower barrier is associated with more complete annealing of the moments into a low energy state.

We next examined the ground state fraction for annealed square artificial spin ice arrays with various thicknesses (15 nm, 20 nm, and 25 nm). We chose these thicknesses to be large enough that the island moments were unaffected by the MFM tip, allowing the moment configuration to be studied after annealing. These are also thicknesses for which T_C appears approximately constant (see Fig. 2). For these measurements, we studied island dimensions of $160 \times 60 \text{ nm}^2$ with gaps of 100 nm, 180 nm, and 280 nm. The postannealing ground state fraction is plotted vs interaction energy in Fig. 5(a), and the energy barriers for various thickness islands are shown in the inset. These data again suggest that the ground state fraction for a given interaction energy strength is correlated with the decrease in the size of the approximate energy barrier to island moment reversal. In fact, the highest ground state fraction in this

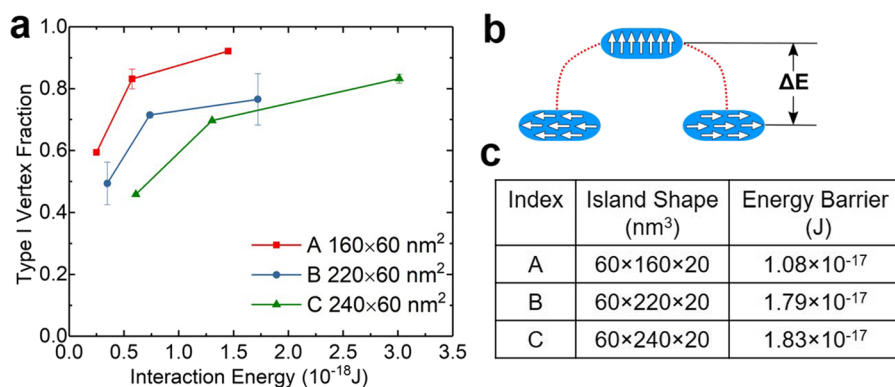


FIG. 4. (a) Island shape-dependence of the ground state fraction on 20-nm-thick lattices with various island shapes and gaps after annealing at 783 K for 10 min. (b) Schematic illustrating how the energy barrier is approximated. (c) Approximate energy barriers for 20 nm-thick and 60 nm-wide islands of various lengths.

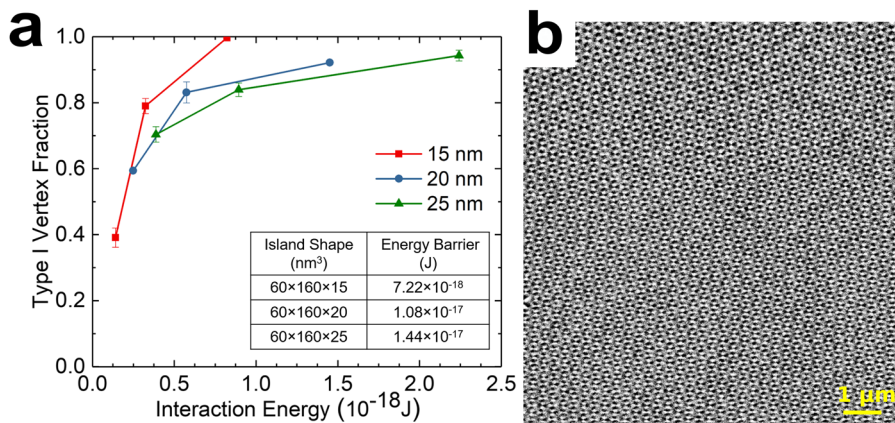


FIG. 5. Thickness-dependent ground state fraction for $160 \times 60 \text{ nm}^2$ square lattices with gaps of 100 nm, 180 nm, and 280 nm after annealing at 783 K for 10 min. The inset table shows the energy barrier for each island thickness. (b) $10 \times 10 \mu\text{m}^2$ MFM image of $160 \times 60 \text{ nm}^2$ island shapes with 100 nm gap and 15 nm thickness. A near-ideal ground state is achieved.

study is seen for the smallest aspect ratio islands with $160 \times 60 \text{ nm}^2$ lateral dimensions, 100 nm gap, and 15 nm thickness, for which an MFM image is shown in Fig. 5(b).

Artificial spin ice systems near their T_C are in a fascinating regime where the magnetization is strongly temperature dependent, with corresponding impacts on both the interisland interactions and the superparamagnetic moment relaxation time. As a result, the collective thermal dynamics of the moments in this regime, and how that relates to the intrinsic frustration for which these systems are designed, cannot be analyzed within a framework of simple superparamagnetic relaxation. Our data on the fraction of ground state vertices serve as a proxy for how well annealing accesses the complex many-body states of artificial spin ice systems. The results indicate that accessing the lowest energy collective states by annealing can be improved by appropriate choice of island shape, spacing, thickness, and annealing temperature but that some systems are not amenable to reaching the lowest possible collective energy state by annealing methods. Previous annealing studies also failed to attain a complete ground state for certain lattices,^{9,12} and the ordered ground state of the kagome lattice has never been achieved by annealing.²⁵ These results suggest that the effectiveness of annealing is limited by local minima in the energy landscape associated with lithographic disorder⁹ and that lithographic perfection might be a limiting factor for this approach. On the other hand, given the complexity of the many-body relaxation process in a system where temperature dependence to relaxation time is associated with multiple factors, we cannot rule out limits associated with the collective relaxation process or very long relaxation time scales that are outside the scope of the present work.

Finally, we note that our results on the strong T_C dependence on the film thickness has implications for other studies of permalloy artificial spin ice and PEEM measurements, in particular, since those measurements appear to be in a regime in which the magnetization has considerable temperature dependence. This regime should thus provide fertile ground for interesting new physical phenomena in nanostructured systems. While we studied only the square ice lattice, we expect these considerations to carry forward to other geometries, opening the possibility of more closely examining low energy states and collective thermal relaxation processes in a range of systems.

See the [supplementary material](#) for the magnetization data for each permalloy film, the residual polarization for MFM images, and the dwell time dependence.

Work at the University of Illinois at Urbana-Champaign and Yale University was funded by the US Department of Energy, Office of Basic Energy Sciences, Materials Sciences and Engineering Division under Grant No. DE-SC0010778. This work was carried out in part in the Frederick Seitz Materials Research Laboratory Central Research Facilities, University of Illinois at Urbana-Champaign. Work at the University of Minnesota was supported by NSF through Grant No. DMR-1807124. The work of C.N. was carried out under the auspices of the US DoE through LANL, operated by Triad National Security, LLC (Contract No. 892333218NCA000001) and financed by DoE LDRD.

REFERENCES

- R. F. Wang, C. Nisoli, R. S. Freitas, J. Li, W. McConville, B. J. Cooley, M. S. Lund, N. Samarth, C. Leighton, V. H. Crespi, and P. Schiffer, "Artificial 'spin ice' in a geometrically frustrated lattice of nanoscale ferromagnetic islands," *Nature* **439**, 303–306 (2006).
- I. Gilbert, C. Nisoli, and P. Schiffer, "Frustration by design," *Phys. Today* **69**(7), 54 (2016).
- M. J. Morrison, T. R. Nelson, and C. Nisoli, "Unhappy vertices in artificial spin ice: New degeneracies from vertex frustration," *New J. Phys.* **15**, 045009 (2013).
- I. Gilbert, G.-W. Chern, S. Zhang, L. O'Brien, B. Fore, C. Nisoli, and P. Schiffer, "Emergent ice rule and magnetic charge screening from vertex frustration in artificial spin ice," *Nat. Phys.* **10**, 670–675 (2014).
- Y. Lao, F. Caravelli, M. Sheikh, J. Sklenar, D. Gardeazabal, J. D. Watts, A. M. Albrecht, A. Scholl, K. Dahmen, C. Nisoli, and P. Schiffer, "Classical topological order in the kinetics of artificial spin ice," *Nat. Phys.* **14**, 723–727 (2018).
- X. Ke, J. Li, C. Nisoli, P. E. Lammert, W. McConville, R. F. Wang, V. H. Crespi, and P. Schiffer, "Energy minimization and ac demagnetization in a nanomagnet array," *Phys. Rev. Lett.* **101**, 037205 (2008).
- J. P. Morgan, A. Stein, S. Langridge, and C. H. Marrows, "Thermal ground-state ordering and elementary excitations in artificial magnetic square ice," *Nat. Phys.* **7**, 75–79 (2011).
- A. Farhan, P. M. Derlet, A. Kleibert, A. Balan, R. V. Chopdekar, M. Wyss, J. Perron, A. Scholl, F. Nolting, and L. J. Heyderman, "Direct observation of thermal relaxation in artificial spin ice," *Phys. Rev. Lett.* **111**, 057204 (2013).
- J. Drisko, S. Daunheimer, and J. Cumings, "FePd₃ as a material for studying thermally active artificial spin ice systems," *Phys. Rev. B* **91**, 224406 (2015).

- ¹⁰S. A. Morley, S. T. Riley, J.-M. Porro, M. C. Rosamond, E. H. Linfield, J. E. Cunningham, S. Langridge, and C. H. Marrows, "Effect of FePd alloy composition on the dynamics of artificial spin ice," *Sci. Rep.* **8**, 4750 (2018).
- ¹¹J. M. Porro, A. Bedoya-Pinto, A. Berger, and P. Vavassori, "Exploring thermally induced states in square artificial spin ice arrays," *New J. Phys.* **15**, 055012 (2013).
- ¹²S. Zhang, I. Gilbert, C. Nisoli, G.-W. Chern, M. J. Erickson, L. O'Brien, C. Leighton, P. E. Lammert, V. H. Crespi, and P. Schiffer, "Crystallites of magnetic charges in artificial spin ice," *Nature* **500**, 553–557 (2013).
- ¹³J. Sklenar, Y. Lao, A. Albrecht, J. D. Watts, C. Nisoli, G.-W. Chern, and P. Schiffer, "Field-induced phase coexistence in an artificial spin ice," *Nat. Phys.* **15**, 191–195 (2019).
- ¹⁴C. Castelnovo, R. Moessner, and S. L. Sondhi, "Spin ice, fractionalization, and topological order," *Annu. Rev. Condens. Matter Phys.* **3**, 35 (2012).
- ¹⁵G. Möller and R. Moessner, "Artificial square ice and related dipolar nanoarays," *Phys. Rev. Lett.* **96**, 237202 (2006).
- ¹⁶G. A. Allan, "Critical temperatures of Ising lattice films," *Phys. Rev. B* **1**, 352 (1970).
- ¹⁷M. E. Fisher and M. N. Barber, "Scaling theory for finite-size effects in the critical region," *Phys. Rev. Lett.* **28**, 1516 (1972).
- ¹⁸Y. Lao, "Study of thermal kinetics in artificial spin ice systems," Ph.D. thesis, University of Illinois at Urbana-Champaign, 2018.
- ¹⁹R. M. Bozorth, *Ferromagnetism* (Wiley, 1993).
- ²⁰D. Mauri, D. Scholl, H. C. Siegmann, and E. Kay, "Magnetism in very thin films of permalloy measured by spin polarized cascade electrons," *Appl. Phys. A* **49**, 439–447 (1989).
- ²¹A. Farhan, A. Kleibert, P. M. Derlet, L. Anghinolfi, A. Balan, R. V. Chopdekar, M. Wyss, S. Gliga, F. Nolting, and L. J. Heyderman, "Thermally induced magnetic relaxation in building blocks of artificial kagome spin ice," *Phys. Rev. B* **89**, 214405 (2014).
- ²²S. Gliga, G. Hrkac, C. Donnelly, J. Büchi, A. Kleibert, J. Cui, A. Farhan, E. Kirk, R. V. Chopdekar, Y. Masaki, N. S. Bingham, A. Scholl, R. L. Stamps, and L. J. Heyderman, "Emergent dynamic chirality in a thermally driven artificial spin ratchet," *Nat. Mater.* **16**, 1106–1111 (2017).
- ²³M. J. Donahue and D. G. Porter, "OOMMF user's guide, version 1.0," Interagency Report No. NISTIR 6376, 1999.
- ²⁴A. Vansteenkiste, J. Leliaert, M. Dvornik, M. Helsen, F. Garcia-Sanchez, and B. V. Waeyenberge, "The design and verification of MuMax3," *AIP Adv.* **4**, 107133 (2014).
- ²⁵L. Anghinolfi, H. Luetkens, J. Perron, M. G. Flokstra, O. Sendetskiy, A. Suter, T. Prokscha, P. M. Derlet, S. L. Lee, and L. J. Heyderman, "Thermodynamic phase transitions in a frustrated magnetic metamaterial," *Nat. Commun.* **6**, 8278 (2015).